JOURNAL OF APPLIED ELECTROCHEMISTRY **16** (1986) 757–767

Indirect electrosynthesis of p-*methoxybenzaldehyde*

G. KREYSA, H. MEDIN*

Dechema-Institute, Theodor-Heuss-Allee 25, 6000 Frankfurt/Main 97, Federal Republic of Germany

Received 19 August 1985; revised 3 December 1985

High current efficiency and selectivity were obtained in the indirect electrochemcial oxidation of *p*-methoxytoluene to *p*-methoxybenzaldehyde with Ce^{4+}/Ce^{3+} as redox mediator system. Platinized titanium anodes can be used for oxidant regeneration. Selectivity of *p*-methoxybenzaldehyde synthesis has been optimized up to 98% by Plackett–Burman and factorial design of experiments. The kinetics of *p*-methoxytoluene oxidation by Ce^{4+} with CH_2Cl_2 as organic solvent has been found to be of mixed mass transfer and kinetic control.

Nomenclature

a_p	specific interfacial area (cm^{-1})
A_p	interfacial area (cm^2)
Ar	aryl group
c	concentration ($mol\,l^{-1}$)
d	diffusion layer thickness (cm)
E	variable effect
E_A	activation energy ($kJ\,mol^{-1}$)
j	material flux ($mol\,s^{-1}$)
k	mass transfer coefficient ($cm\,s^{-1}$)
n	molar amount (mol)
n^0	starting molar amount (mol)
n^{rel}	relative molar amount
Q_r	relative amount of charge
Q_{th}	theoretical amount of charge
r	reaction rate ($mol\,l^{-1}\,s^{-1}$)
r^0	initial reaction rate ($mol\,l^{-1}\,s^{-1}$)
S	overall selectivity
T	temperature (K)
X	fractional conversion
ν	stoichiometric coefficient
ϕ^e	current efficiency
θ	overall operational yield
dim	dimerization product of *p*-MT

1. Introduction

Since any electrochemical reaction is a redox reaction, most of the electro-organic reactions of industrial interest [1–4] can be performed not only directly at the electrode but also in an indirect manner employing a chemical redox system which reacts with the substrate and is then regenerated electrochemically. An indirect electrolysis may be advantageous in some of the following situations

(i) where there is low solubility of the substrate in aqueous electrolyte,

(ii) where costly conducting salt is necessary for an electrolysis in the organic phase,

(iii) where the wanted product is not stable against further electrochemical conversion.

The problems arising in designing an indirect electrochemical process, in fitting the electrochemical and chemical step together and in optimization of yields and selectivity are discussed in the present paper for the example of indirect electrosynthesis of *p*-methoxybenzaldehyde (*p*-MBA) by oxidation of *p*-methoxytoluene (*p*-MT). The feasibility of indirect electrolytic oxidation of aromatic compounds to aldehydes has already been proven by other authors [5–11] employing Mn^{3+} and Ce^{4+} as oxidizing agents. The electrolytic regeneration of these redox systems has also been investigated [12, 13].

The aldehyde *p*-MBA (anisaldehyde) is a natural constituent of some etheric oils and is used as a flavour component of soaps and other cosmetics and as an intermediate for the synthesis of some pharmaceuticals. Chemical

* *Present address*: Hökvägen 6, S-22232 Lund, Sweden.

0021–891X/86 $03.00 + .12

syntheses of this aldehyde are, for example, the oxidation of *p*-methoxystyrene, the formylation of methoxybenzene or the methylation of *p*-hydroxybenzaldehyde [14]. Electrochemical processes for *p*-MBA including direct electrolysis at graphite electrodes [15–17] and indirect electrolysis with Mn^{3+} [18, 19] have been described in the patent literature.

The purpose of the present paper is to introduce an indirect electrochemical process for the oxidation of *p*-MT to *p*-MBA. Mn^{3+} and Ce^{4+} have been tested as redox mediator systems. The electrochemical and the chemical step have been investigated separately in order to determine operating conditions providing a high current efficiency and selectivity [20].

2. Experimental details

The electrochemical oxidation experiments with Mn^{2+} (0.1 M Mn^{2+} in 4.5 M H_2SO_4) and Ce^{3+} (0.2 M Ce^{3+} in 1 M H_2SO_4) were performed in an undivided cell using a platinum wire as cathode. The anode materials are listed in Table 1. Current efficiencies for Mn^{2+} and Ce^{3+} oxidation at these materials were determined by steady-state polarization curves measured with and without metal ion substrate and by galvanostatic experiments. The galvanostatic oxidations were performed at two different stirring rates (300 and 800 r.p.m.) and a relative amount of charge ($Q_r = Q/Q_{th}$) of 50%. The current efficiencies, ϕ^e, were determined by titration with iron(II)

Table 1. Current efficiencies for Mn^{2+} and Ce^{3+} oxidation in sulphuric acid (0.2 M Ce^{3+} + 1 M H_2SO_4 and 0.1 M Mn^{2+} + 4.5 M H_2SO_4) at two stirring rates

Electrode	i *(A dm^{-2})*	*Ce^{3+}*		*Mn^{2+}*	
		300 r.p.m.	*800 r.p.m.*	*300 r.p.m.*	*800 r.p.m.*
Platinum	2	0.91	–	–	0.85
	4	0.68	0.94	0.50	0.62
	5	–	0.83	–	–
	6	0.59	0.71	–	–
PbO_2/Ti[a] [21]	2	0.77	–	–	–
	2.5	0.69	–	0.85	–
	3	–	0.85	–	0.91
	4	0.50	0.77	–	0.92
	6	–	0.66	–	0.86
DSA I[b] (coated with platinates and non-stoichiometric ruthenium compounds)					
	1.5	0.65	0.75	–	–
	3	0.48	0.61	0.12	–
DSA II[b] (coated with platinates and platinum)					
	1.5	–	0.84	–	–
	2	–	–	0.15	–
	2.25	0.63	–	–	–
	3	0.57	0.78	–	–
DSA III[b] (coated with non-stoichiometric platinum and iridium compounds)					
	1.5	–	0.82	–	–
	2	0.67	0.86	0.18	–
	3	0.55	0.81	–	–
DSA IV[b] (coated with non-stoichiometric ternary iridium compounds)					
	1.5	–	0.85	–	–
	1.8	0.72	–	–	–
	3	0.56	0.81	0.15	–

[a] Provided by Priv.-Doz. Dr D. W. Wabner, TU München, West Germany.
[b] Provided by C. Conradty GmbH, Nürnberg, West Germany.

sulphate in 4.5 M H_2SO_4 using ferroin as indicator. The experiments for the chemical oxidation of *p*-MT were conducted in a three-necked flask submerged in a constant-temperature bath. The flask was equipped with a condenser, a thermometer and a stirrer (225 r.p.m.) or dispergator (10 000 r.p.m.). The experiments were started by adding the organic phase to the aqueous phase. After reaction the phases were separated and the aqueous phase was extracted with methylene chloride. The combined organic phases were dried over Na_2SO_4. The concentrations of the products and unconverted substrate were determined by gas chromatography using *p*-dimethoxybenzene as internal standard.

All chemicals, except manganese(III) sulphate, were used as commercially available p.a. grade substances. The Mn^{3+} solution was produced electrochemically from manganese(II) sulphate and was filtered and titrated before use.

3. Results and discussion

3.1. *The electrochemical step*

The galvanostatically determined integral current efficiencies for Mn^{2+} and Ce^{3+} oxidation in sulphuric acid at various electrode materials are summarized in Table 1. These experiments were conducted in an undivided cell with a high anode to cathode surface area ratio, a design concept which has also been applied by Ibl and co-workers [11] for Ce^{3+} oxidation in order to obtain a high anodic current efficiency. The results in Table 1 show that the current efficiency for both metal ion oxidations increased with increasing stirring rate and decreasing current density. This indicates a mainly diffusion-controlled electrode reaction.

The most suitable electrode material for Ce^{3+} oxidation is platinum (or platinum-coated titanium as used by Ibl and co-workers [11]); this provided a current efficiency of 94% at 4 A dm^{-2}. For Mn^{2+} oxidation a current efficiency of 92% at 4 A dm^{-2} was obtained at PbO_2–Ti anodes. This means that, based on these data, no decision can be made as to whether *p*-MT should be preferably oxidized using Mn^{3+} or Ce^{4+}. Electrochemical regeneration is possible for both systems with comparable efficiency.

3.2. *The chemical step — factorial design experiments*

The oxidation of *p*-MT proceeds schematically as a sequence of consecutive reaction steps.

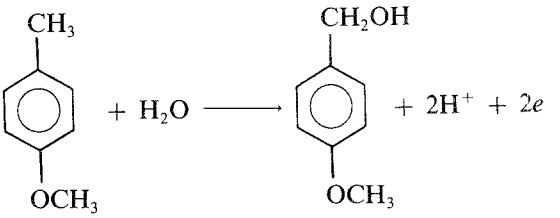

(1)

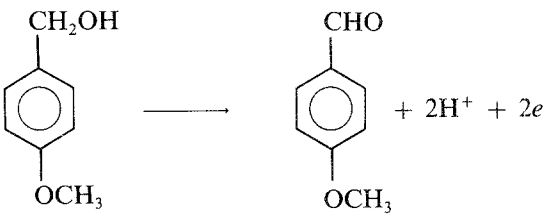

(2)

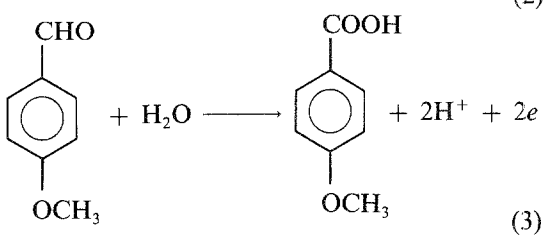

(3)

Apart from this sequence *p*-MT can undergo an anodic or oxidative oligomerization which can be formulated for the dimerization as follows.

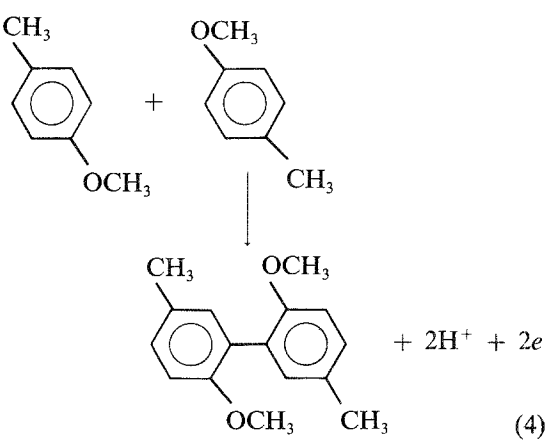

(4)

This dimerization product has been found as a by-product of *p*-MT oxidation with Ce^{4+} and is probably formed via a cation radical mechanism [22, 23].

Assuming that the alcohol oxidation is a fast reaction because the alcohol is not a stable intermediate and that the oligomerization as a side reaction producing mainly dimers, the reactions 1–4 may be summarized according to the following scheme of *p*-MT oxidation by a metal ion transferring one electron.

$$p\text{-MT} \begin{cases} \xrightarrow{4Me^{z+}} p\text{-MBA} \xrightarrow{2Me^{z+}} p\text{-MBAc} \\ \xrightarrow{Me^{z+}} \tfrac{1}{2}(p\text{-MT})_2 \end{cases} \quad (5)$$

with

$$Me^{z+} + e \longrightarrow Me^{(z-1)+}$$

The evaluation of the experimental conversion data is based on this reaction scheme. The following quantities can be defined.

Fractional conversion:

$$X_{p\text{-MT}} = 1 - \frac{n_{p\text{-MT}}}{n^0_{p\text{-MT}}} \quad (6)$$

Overall operational yield related to oxidant consumption:

$$\theta_{p\text{-MBA}} = \frac{n_{p\text{-MBA}}\, \nu_{Me^{z+}}}{(n^0_{Me^{z+}} - n_{Me^{z+}})} \quad (7)$$

Overall product selectivities:

$$S_p = \frac{n_p/\nu_p}{n^0_{p\text{-MT}}\, X_{p\text{-MT}}} \quad (8)$$

In some cases the relative molar amount of the applied oxidant is given as an additional experimental parameter.

$$n^{rel}_{Me^{z+}} = \frac{n^0_{Me^{z+}}}{4n^0_{p\text{-MT}}} \quad (9)$$

The following experimental investigations were carried out in order to find operating conditions that provide a maximum aldehyde selectivity.

Comparative preliminary experiments were conducted in *p*-MT oxidation with Ce^{4+} and Mn^{3+} with a relative amount of oxidant of 0.8. Experiments were run to complete oxidant consumption. The results are listed in Table 2. The high concentration of sulphuric acid was chosen in order to avoid disproportionation of Mn^{3+}. Because Ce^{4+} provides a somewhat better aldehyde selectivity further studies were restricted to this system.

A factorial design method introduced originally by Plackett and Burman [24, 25] was used for screening seven variables in the *p*-MT oxidation reaction in order to select the more important ones using only eight experiments. A complete factorial design at two levels would require 128 experiments. The Plackett–Burman (PB) design was carried out twice; with n-hexane and with methylene chloride as solvent in the organic phase. The seven variables, their low and high levels and their effects on the *p*-MBA selectivity are listed in Table 3. The layout of the PB design and the determined *p*-MBA selectivities for each of the eight runs with n-hexane and CH_2Cl_2 as solvent are given in Table 4. The effects of the variables on the selectivity were calculated according to

$$E_s = \overline{S^{(+)}_{p\text{-MBA}}} - \overline{S^{(-)}_{p\text{-MBA}}} \quad (10)$$

as difference between the mean values at high and low levels. The selectivity effects in Table 3 indicate that the concentrations of Ce^{3+} and H_2SO_4 in the aqueous phase, the *p*-MT concentration in the organic phase and the degree of dispersion are the most important parameters. No remarkable difference between the two solvents can be detected. The only significant

Table 2. Comparative oxidation of p-*MT by* Ce^{4+} *and* Mn^{3+}

Oxidant	$n^0_{p\text{-MT}}$ *(mmol)*	$X_{p\text{-MT}}$	$\theta_{p\text{-MBA}}$	$S_{p\text{-MBA}}$	$S_{p\text{-MBAc}}$	S_{dim}
Ce^{4+}	19.4	0.82	0.74	0.72	0.15	0.13
Mn^{3+}	33.0	0.92	0.36	0.31	0.31	0.38

$T = 35°$ C; solution stirred, 225 r.p.m. Organic phase: 0.721 mol l^{-1} *p*-MT in CH_2Cl_2 (27 and 45.8 ml, respectively). Aqueous phase: 68.89 mmol l^{-1} Ce^{4+} in 4.5 mol l^{-1} H_2SO_4 (500 ml); 117.8 mmol l^{-1} Mn^{3+} in 4.5 mol l^{-1} H_2SO_4 (500 ml).

Table 3. Variables, levels and selectivity effects of the Plackett–Burman design

Code	*Variable*	*Low level*	*High level*	*Selectivity effects,* E_s	
				n-Hexane	CH_2Cl_2
A	C_{Ce3+} ($mol\,l^{-1}$)	0	0.1	−0.18	−0.18
B	$C_{H_2SO_4}$ ($mol\,l^{-1}$)	0.5	3	−0.21	−0.18
C	$C_{p\text{-MT}}$ (n-hexane) ($mol\,l^{-1}$)	pure	0.496	0.29	
	$C_{p\text{-MT}}(CH_2Cl_2)$ ($mol\,l^{-1}$)	pure	0.721		0.33
D	Dispersion	low[a]	high[b]	−0.18	−0.14
E	$n^0_{p\text{-MT}}$ (mmol)	20	50	0	0
F	T(n-hexane) (°C)	25	50	−0.07	
	$T(CH_2Cl_2)$ (°C)	25	35		0.06
G	C_{Ce4+} ($mol\,l^{-1}$)	0.05	0.15	0.07	0.01

[a] Stirrer: 225 r.p.m., $a_p = 51\,cm^{-1}$.
[b] Dispergator: 10 000 r.p.m., $a_p = 730\,cm^{-1}$.
Reaction time to oxidant conversion.

difference shows the temperature effect which may be due to the different high levels of this variable used for the two solvents. In general, cautious interpretation of these results is necessary since the main effects may also be influenced by two-factor, three-factor and higher order interactions. Experiments 2 and 18 in Table 4, which were run without solvent at the same temperature, demonstrate the reproducibility since they are identical for both solvents.

The selectivity data in Table 4 show that methylene chloride provides a higher mean selectivity than n-hexane. This is due to the higher solubility of *p*-MBA in CH_2Cl_2 which corresponds to a lower concentration of *p*-MBA in the aqueous phase. Therefore, in the methylene chloride system the *p*-MBA is better protected against further oxidation to *p*-MBAc by re-extraction. This explanation is supported by the experimental finding that the current efficiency of Ce^{3+} oxidation in the presence of *p*-MBA is lower in an electrolyte in contact with a n-hexane phase loaded with *p*-MBA than in contact with CH_2Cl_2.

A question which is not clearly answered by the PB design is the effect on selectivity of the relative amount of Ce^{4+}. Three experiments related to this point are listed in Table 5. All these tests were run to complete consumption of the oxidant. These results indicate that the p-MBA selectivity decreases with increasing relative molar amount of Ce^{4+}. The reaction

Table 4. Plackett–Burman matrix for seven variables

Run	*Variable*							$S_{p\text{-MBA}}/I$	
	A	*B*	*C*	*D*	*E*	*F*	*G*	*n-Hexane*	CH_2Cl_2
1	+	+	+	−	+	−	−	0.64	0.70
2	+	+	−	+	−	−	+	0.24	0.25
3	+	−	+	−	−	+	+	0.85	0.95
4	−	+	−	−	+	+	+	0.54	0.61
5	+	−	−	+	+	+	−	0.31	0.47
6	−	−	+	+	+	−	+	0.92	0.93
7	−	+	+	+	−	+	−	0.57	0.80
8	−	−	−	−	−	−	−	0.74	0.73
							mean value	0.60	0.68

−, Low level; +, high level.

Table 5. Influence of relative amount of Ce^{4+}

n^{rel}_{Ce4+}	$n^{0}_{p\text{-}MT}$ *(mmol)*	t *(h)*[a]	$X_{p\text{-}MT}$	$S_{p\text{-}MBA}$	$S_{p\text{-}MBAc}$	S_{dim}
0.55	25	1.5	0.45	0.95	0.05	0
0.99	50	4	0.96	0.90	0.08	0.02
1.10	37.5	15	1.00	0.86	0.14	0

[a] Reaction time to complete oxidant consumption.
$T = 40°C$; solution stirred, 225 r.p.m. Organic phase: 2.266 mol l^{-1} *p*-MT in CH_2Cl_2 (11, 22 and 16.6 ml, respectively). Aqueous phase: 220 mmol l^{-1} Ce^{4+} in 1 mol l^{-1} H_2SO_4 (500 ml).

times also show that *p*-MBA oxidation to *p*-MBAc is slow compared to *p*-MBA formation.

Based on the results of the PB design a complete factorial design [26] was carried out with a reduced number of variables. These variables and their levels are listed in Table 6. The reasons for choosing these variables and levels are as follows. The concentrations of H_2SO_4 and *p*-MT were suggested as being important by the PB design. The levels of $c_{p\text{-}MT}$ are lower and higher than the optimum value of the PB design. The high level of $c_{H_2SO_4}$ has been reduced because a lower acid concentration increases the selectivity. The levels of $c_{Ce^{3+}}$ were chosen around the high level of the PB design. To also include zero Ce^{3+} content into the factorial design, as is suggested by the negative selectivity effect of the PB design, seemed to be unreasonable since this would be only typical for the beginning of the reaction between Ce^{4+} and *p*-MT when the spent redox electrolyte is completly regenerated. Ce^{4+} was also included at the same levels as Ce^{3+}. Temperature was kept constant at the high level and dispersion at the low level as suggested by the results of the PB design. The value of $n^{0}_{p\text{-}MT}$ was chosen depending on c_{Ce4+} is such a way that n^{rel}_{Ce4+} was constant at 0.8 as recommended by the results in Table 5. All 16 experiments were run with an aqueous phase of 500 ml to complete oxidant consumption. The selectivity results of the factorial design are listed in standard order in Table 7. Statistical evaluation of these data shows that no significant interactions exist. The main parameter effects are given in Table 8.

Table. 6. Variables and levels of the factorial 2^4 design

Code	*Variable* *(mol l^{-1})*	*Low level*	*High level*
A	C_{Ce3+}	0.05	0.15
B	C_{Ce4+}	0.05	0.15
C	$C_{p\text{-}MT}$	0.496	1.322
D	$C_{H_2SO_4}$	0.5	1.5

To aid further discussion the distribution coefficient of *p*-MT between pure water and CH_2Cl_2 was measured as

$$K_p = \frac{C^{org}_{p\text{-}MT}}{C^{aqu}_{p\text{-}MT}} = 6.7 \times 10^3$$

The solubility of pure *p*-MT in an aqueous solution as a function of the concentrations of H_2SO_4 and $Ce_2(SO_4)_3$ is shown in Fig. 1.

Taking the information provided by the PB and the factorial design together, the following conclusions can be drawn. The *p*-MBA selectivity seems to be mainly determined by the aqueous *p*-MT concentration because the low

Table 7. Results of the factorial 2^4 design

Run	$S_{p\text{-}MBA}$ *(%)*	$S_{p\text{-}MBAc}$ *(%)*	S_{dim} *(%)*
(1)	95.5	2.3	2.2
a	94.0	3.1	2.9
b	98.0	1.5	0.5
ab	98.3	1.2	0.5
c	94.4	0.5	5.1
ac	95.4	0	4.8
bc	96.3	1.9	1.8
abc	96.8	1.8	1.4
d	96.5	1.1	2.4
ad	95.4	2	2.6
bd	97.7	1.4	0.9
abd	97.9	1.3	0.8
cd	94.9	0.7	4.4
acd	94.5	1.3	4.2
bcd	96.1	1.9	1.9
abcd	96.7	1.6	1.7

Table 8. Main parameter effects (%) of the 2^4 design

Effected quantity	*Variables*			
	c_{Ce3+}	c_{Ce4+}	$c_{p\text{-MT}}$	$c_{H_2SO_4}$
$S_{p\text{-MBA}}$	NS	2.15	−1.03	NS
$S_{p\text{-MBAc}}$	NS	NS	NS	NS
S_{dim}	NS	−2.39	+1.56	NS

NS, not significant.

solubility of Ce^{4+} in the organic phase supports the assumption that the oxidation takes place in the aqueous phase. Since the dimerization proceeds with a higher formal *p*-MT reaction order a high *p*-MT concentration favours the dimerization whereas an increasing Ce^{4+} concentration supports the oxidation. Based on the supposed cation radical mechanism of dimerization [22, 23] a high acid concentration stabilises the benzyl radical which undergoes dimerization. A low proton concentration favours the formation of the deprotonated radical which can easily be oxidized.

$$Ar{-}CH_3^{\cdot+} \rightleftharpoons Ar{-}CH_2\cdot + H^+ \quad (11)$$

The influence of the Ce^{3+} concentration may be a competitive one. On the one hand a high Ce^{3+} concentration decreases the *p*-MT solubility according to Fig. 1 which should increase the *p*-MBA selectivity, whereas on the other hand the oxidation potential of Ce^{4+}/Ce^{3+} decreases with increasing Ce^{3+} concentration which may support the dimerization. The influence of the interfacial area (see Table 3) indicates that the reaction kinetics may be partially mass transfer controlled. An enlarged a_p increases the mass transfer rate resulting in an increased steady state aqueous *p*-MT concentration decreasing the *p*-MBA selectivity. To test some of these ideas an additional kinetic study of the *p*-MT oxidation by Ce^{4+} was carried out.

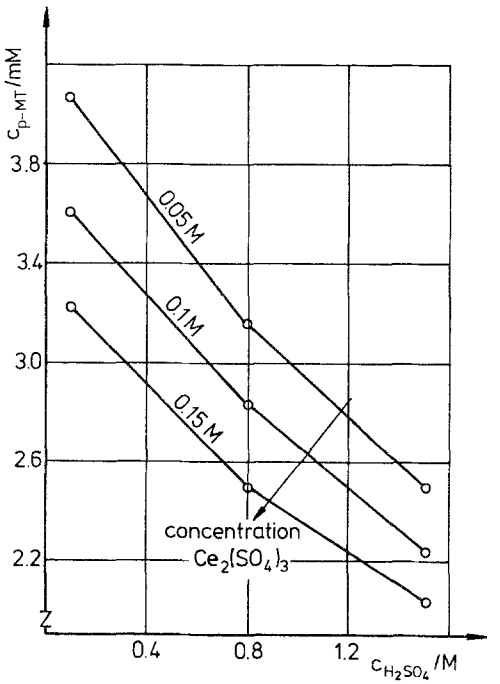

Fig. 1. Solubility of *p*-MT in aqueous solutions at 22° C.

3.3. *Chemical step — kinetic study*

In a stirred vessel (225 r.p.m.) the organic phase was added to 900 ml of the aqueous phase. At intervals of 30 min, stirring was interrupted for 1 min to allow phase separation. In a 10 ml sample of the aqueous phase the Ce^{4+} concentration was determined by titration with $FeSO_4$ using ferroin as indicator. Further experimental conditions are given in Table 9. The concentration time functions obtained are shown in Figs 2 and 3.

For the interpretation of these results a model has been established based on the film theory, assuming that the main mass transfer resistance is located in the aqueous phase. A schematic presentation of the interfacial concentration profile is given in Fig. 4. The *p*-MT flux across the interface may be written as

Table 9. Conditions of the kinetic experiments

Run	$c_{H_2SO_4}$ *(mol l^{-1})*	$c_{p\text{-MT}}$ *(mol l^{-1})*	T *(° C)*	V_{org} *(ml)*
1	1.5	1.322	35	227.3
2	1.5	1.322	5	227.3
3	0.5	1.322	5	227.3
4	1.5	0.496	35	201.6
5	1.5	0.496	20	201.6
6	0.5	0.496	20	201.6

Organic phase: *p*-MT in CH_2Cl_2.
Aqueous phase: 900 ml 0.15 mol l^{-1} $Ce(SO_4)_2$ + 0.025 mol l^{-1} $Ce_2(SO_4)_3$ in aqueous H_2SO_4.

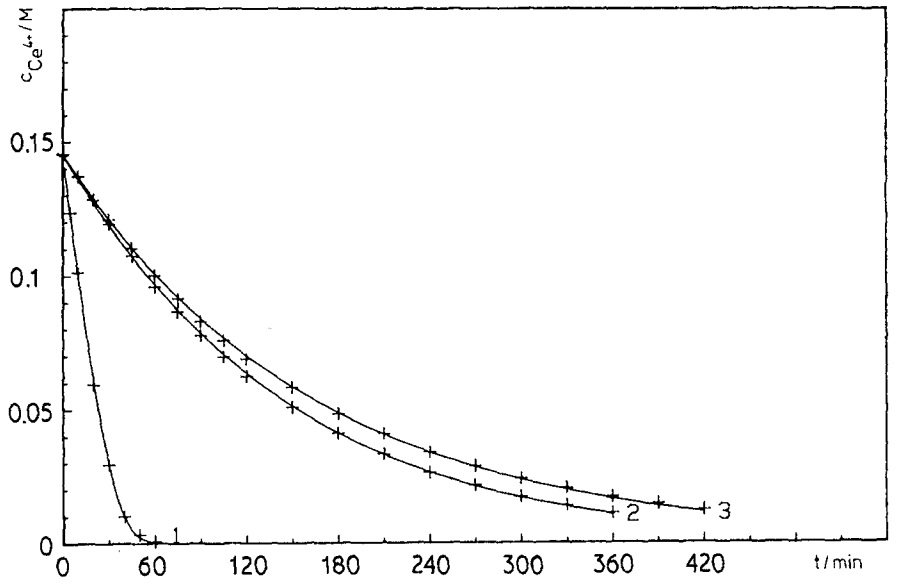

Fig. 2. Concentration–time functions of *p*-MT oxidation by Ce^{4+} (+, experimental data; ——, fitted curves; curve numbers indicate the runs in Table 10).

$$j_{p\text{-MT}} = k_p A_p \left(\frac{C^{org}_{p\text{-MT}}}{K_p} - c^{aqu}_{p\text{-MT}} \right) \quad (12)$$

Assuming that the first electron transfer is the rate determining step for *p*-MT oxidation the reaction rate for *p*-MT is given by

$$r_{p\text{-MT}} = -k c^{aqu}_{p\text{-MT}} c_{Ce^{4+}} \quad (13)$$

Mass transfer flux and reaction rate are linked with the *p*-MT concentration transient in the aqueous phase by the mass balance

$$\frac{dc^{aqu}_{p\text{-MT}}}{dt} = \frac{j_{p\text{-MT}}}{V_{aqu}} + r_{p\text{-MT}} \quad (14)$$

Introducing Equations 12 and 13 into Equation

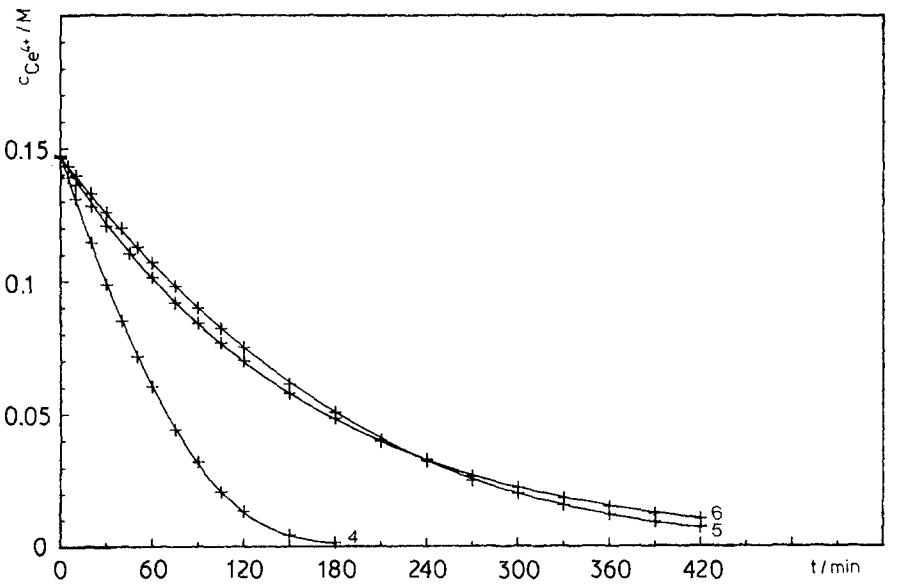

Fig. 3. Concentration–time function of *p*-MT oxidation by Ce^{4+} (+, experimental data; ——, fitted curves; curve numbers indicate the runs in Table 10).

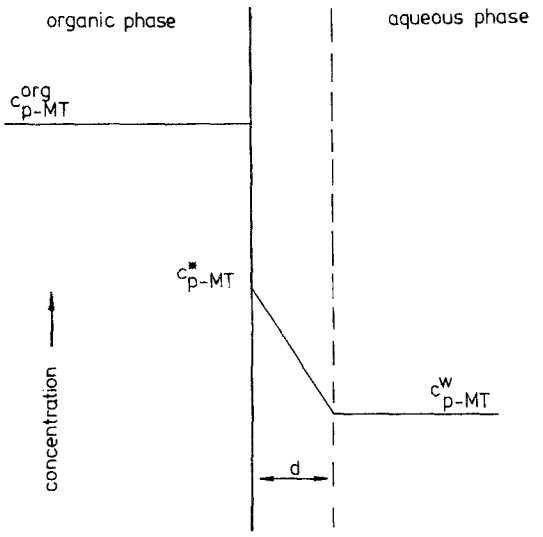

Fig. 4. Schematic concentration profile across the liquid–liquid interface.

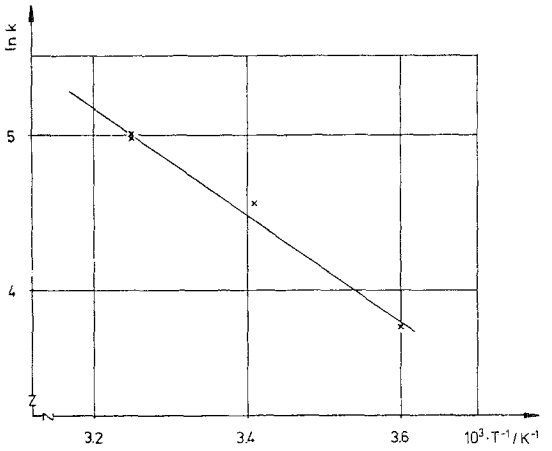

Fig. 5. Arrhenius plot of the rate constants obtained for 1.5 mol l^{-1} H_2SO_4.

14 yields the differential equation

$$\frac{dc^{aqu}_{p\text{-MT}}}{dt} = \frac{k_p A_p}{V_{aqu}}\left(\frac{c^{org}_{p\text{-MT}}}{K_p} - c^{aqu}_{p\text{-MT}}\right) - K c^{aqu}_{p\text{-MT}}\, c_{Ce^{4+}} \quad (15)$$

The *p*-MT concentration change in the organic phase is then given by

$$\frac{dc^{org}_{p\text{-MT}}}{dt} = -\frac{k_p A_p}{V_{org}}\left(\frac{c^{org}_{p\text{-MT}}}{K_p} - c^{aqu}_{p\text{-MT}}\right) \quad (16)$$

Assuming that only *p*-MBA is formed the concentration change of Ce^{4+} in the aqueous phase may be written as

$$\frac{dc_{Ce^{4+}}}{dt} = -4k c^{aqu}_{p\text{-MT}}\, c_{Ce^{4+}} \quad (17)$$

The time-dependence of the three unknown concentrations $c_{Ce^{4+}}$, $c^{org}_{p\text{-MT}}$ and $c^{aqu}_{p\text{-MT}}$ is determined by the three differential equations, 15–17. This system of equations was solved numerically by the Runge–Kutta method [27], whereas the volumetric mass transfer coefficient, $k_p A_p$, the distribution coefficient, K_p and the rate constant, k, were fitted to the experimental results in Figs 2 and 3 by the Simplex method [28]. The results of these parameter fits are given in Table 10. The calculated curves in Figs 2 and 3 show that they fit the experimental data very well. However, such a parameter fitting procedure alone does not prove the model. Additionally the parameter values obtained have to follow physically reasonable trends. Runs 1, 2, 4 and 5 are carried out at the same acid conentration but different temperatures and *p*-MT concentrations. The rate constants determined from these experiments should satisfy an Arrhenius plot as shown in Fig. 5. From this an activation energy of 29 kJ mol^{-1} results. From Fig. 1 it can be concluded that the *p*-MT solubility in the aqueous phase decreases with increasing ionic strength. This explains the K_p increase with increasing sulphuric acid concentration. The temperature dependence of K_p suggests a positive temperature coefficient of the aqueous *p*-MT

Table 10. Results of the kinetic experiments

Run	$-r^0_{Ce^{4+}}$ ($\times 10^5$ *mol* l^{-1} s^{-1})	$k_p A_p$ ($\times 10^{-3}$ *cm*^{3} *min*$^{-1}$)	K_p ($\times 10^{-3}$ *v*)	k ($l mol^{-1} s^{-1}$)
1	8.111	4.3	4.0	148.1
2	1.565	20.9	26.4	42.8
3	1.593	29.7	14.5	18.3
4	3.027	4.6	4.3	146.7
5	1.241	7.5	13.2	95.2
6	1.685	9.8	7.1	33.0

solubility which seems reasonable. The volumetric mass transfer coefficient decreases with increasing sulphuric acid concentration. The same behaviour of the k_pA_p decrease with increasing electrolyte concentration has also been observed in other extraction systems, e.g. CCl_4, J_2/H_2O, KJ [29]. The k_pA_p decrease with increasing temperature may be due to a decreased interfacial area by enhanced coalescence of the droplets. This behaviour of the fitted parameters supports the reliability of the suggested kinetic model.

From the kinetic and mass transfer data in Table 10, Hatta numbers between 0.02 and 0.3 can be estimated for the various runs. This means that the overall kinetics are only weakly influenced by the diffusion rate. The values of the mass transfer coefficient obtained by an estimation of the interfacial area suggest that 99% of equilibrium is established within a time range of 0.1–1 s.

4. Conclusions

Based on electrochemical experiments, factorial design and kinetic studies it has been shown that *p*-MBA can be produced with high selectivity from *p*-MT in an indirect electrochemical process applying Ce^{4+}/Ce^{3+} as the redox mediator system. Because the electrochemical regeneration in the presence of the organic phase suffers from the formation of oligomer layers at the electrodes, an outer cell process is suggested which means that the spent redox electrolyte is separately regenerated and the chemical reaction takes place in another reactor outside of the electrochemical cell.

A schematic flow sheet for a plant producing 10 tonnes per year is shown in Fig. 6. The process data are based on the results of the present investigation. The *p*-MBA can be separated by extraction of the organic phase with an aqueous $NaHSO_3$ solution. From the precipitated sulphonic acid salt of *p*-MBA the product can be recovered using an acid. SO_2 is formed which can react with NaOH to produce $NaHSO_3$ [30].

The kinetic study of *p*-MT oxidation by Ce^{4+} has shown that the reaction rate is determined by a combined mass transfer and kinetic control.

Acknowledgements

The authors wish to thank AIF Arbeitsgemeinschaft Industrieller Forschungsvereinigungen for financial support of this work. The investigations were initiated by Professor Dr E. Heitz, Dechema-Institute and Doz. Dr K. Nyberg, Karlskoga, Sweden, and their helpful discussions are gratefully acknowledged.

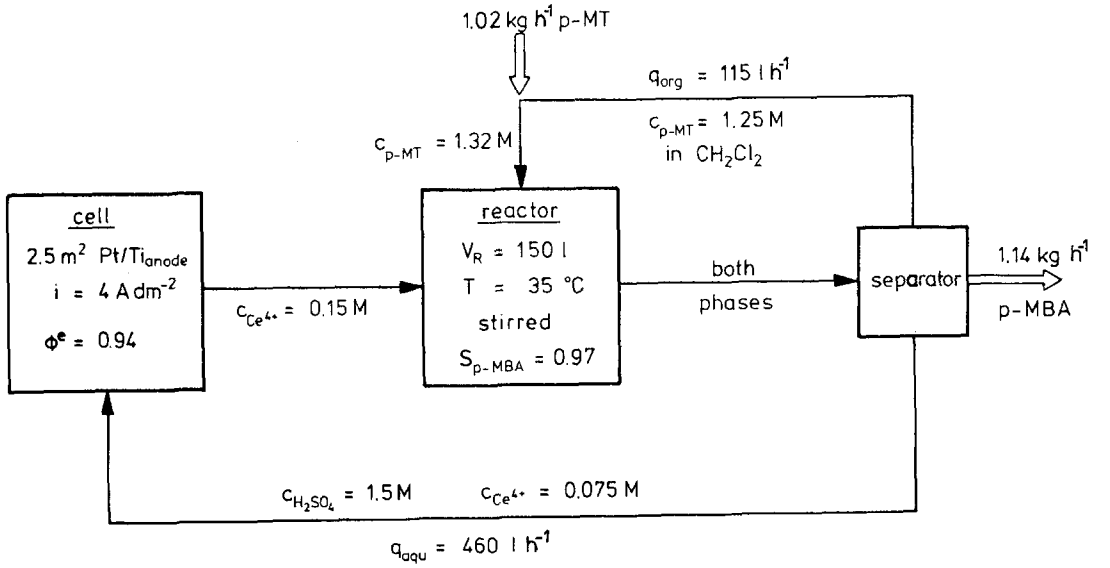

Fig. 6. Schematic process flow sheet for a production rate of 10 tons per year of *p*-MBA.

References

[1] D. Pletcher, *Chem. and Ind.* (1982) 358.
[2] D. Degner, in 'Techniques of Chemistry' (edited by N. L. Weinberg and B. V. Tilak), John Wiley, New York (1982). p. 251.
[3] R. E. W. Jansson, *Chem. Eng. News* **43** (1984).
[4] R. Clarke, A. T. Kuhn and E. Okoh, *Chem. in Brit.* **11**(2) (1975) 59.
[5] M. S. Venkatachalapathy, R. Ramaswamy and H. V. K. Udupa, *Bull. Acad. Polon. Sci. Ser. Sci. Chim.* **8** (1960) 361.
[6] R. Ramaswamy, M. S. Venkatachalapathy and H. V. K. Udupa, *J. Electrochem. Soc.* **110** (1963) 202.
[7] S. Chidambaran, M. S. V. Pathy and H. V. K. Udupa, *J. Electrochem. Soc. India* **17** (1968) 95.
[8] R. Ramaswamy, M. S. Venkatachalapathy and H. V. K. Udupa, *Bull. Chem. Soc. Jpn.* **35** (1962) 1751.
[9] W. S. Trahanovsky and L. B. Young, *J. Org. Chem.* **31** (1966) 2033.
[10] L. Syper, *Tetrahedron Lett.* **37** (1966) 4493.
[11] K. Kramer, P. M. Robertson and N. Ibl, *J. Appl. Electrochem.* **10** (1980) 29.
[12] A. J. Fenton and N. H. Furman, *Anal. Chem.* **32** (1960) 748.
[13] G. F. Smith, G. Frank and A. E. Kott, *Ind. Eng. Chem. Anal. Ed.* **12** (1940) 268.
[14] Ullmanns Encyklopädie der technischen Chemi, 4th ed., Vol. 20, Verlag Chemie, Weinheim (1981) p. 244.
[15] Ger. Offen. 2848397 (1980).
[16] Ger. Offen. 2851732 (1980).
[17] Ger. Offen. 2912058 (1980).
[18] US Patent 4212711 (1980).
[19] Ger. Offen. 2435985 (1975).
[20] H. Medin, Dissertation, TU München 1983.
[21] D. W. Wabner, H.-P. Fritz and R. Huß, *Chem.-Ing.-Tech.* **49**(1977) 329.
[22] R. O. C. Norman, C. B. Thomas and P. J. Ward, *J. Chem. Soc. Perkin I* **23** (1973) 2914.
[23] S. Uemara, T. Ikeda, S. Tanaka and M. Okano, *J. Chem. Soc. Perkin I* **10** (1979) 2574.
[24] R. A. Stowe and R. P. Mayer, *Ind. Eng. Chem.* **58** (1966) 36.
[25] R. L. Plackett and J. P. Burman, *Biometrica* **33** (1946) 305.
[26] O. L. Davies, 'The Design and Analysis of Industrial Experiments', Longman Group, London (1978) pp. 247–89.
[27] W. Törnig, 'Numerische Mathematik für Ingenieure und Physiker', Springer-Verlag, Berlin (1979) p. 162.
[28] R. R. Ernst, *Rev. Sci. Instrum.* **39** (1968) 998.
[29] G. Kreysa and C. Woebcken, *Chem. Eng. Sci.* **41** (1986) 307.
[30] G. V. Jeffreys and G. A. Davies, in 'Recent Advances in Liquid–Liquid Extraction' (edited by C. Hanson), Pergamon Press, Oxford (1971) p. 495.